

Research Article

Characterization of Oxide Growth on Surface of Al-Mg-Si Welded Joint

Azman Jalar,¹ Nur Azida Che Lah,^{1,2} Norinsan Kamil Othman,¹ Roslinda Shamsudin,¹ Abdul Razak Daud,¹ and Syed Roslee Sayd Bakar³

¹ School of Applied Physics, Faculty of Science and Technology, Universiti Kebangsaan Malaysia, 43600 Bangi, Selangor, Malaysia

² Fabrication & Joining Section, Universiti Kuala Lumpur Malaysia France Institute, Section 14, Jalan Teras Jernang, 43650 Bandar Baru Bangi, Selangor, Malaysia

³ Science and Technology Research Institute for Defence (STRIDE), 43000 Kajang, Selangor, Malaysia

Correspondence should be addressed to Azman Jalar; azmn@ukm.my

Received 13 May 2013; Revised 3 December 2013; Accepted 5 December 2013; Published 16 February 2014

Academic Editor: Pavel Lejcek

Copyright © 2014 Azman Jalar et al. This is an open access article distributed under the Creative Commons Attribution License, which permits unrestricted use, distribution, and reproduction in any medium, provided the original work is properly cited.

Al-Mg-Si (AA6061) Al alloy plates were joined by the method of gas metal arc welding using Al-5Mg (ER5356) filler metal and were subjected to the oxidation test in flowing air environment at 600°C from 8 to 40 hours and the weight gain was measured. The characteristic of oxide grown on welded zone surface was examined by SEM/EDS, XRD, and XPS. Oxide was observed to grow on the fused metal surface suggesting the possibility of modifying the oxide chemistry under high temperature environment. It was found that the oxidation behavior of fused metal affected by the nature of their oxide growth and morphology, was influenced by their welding process and the difference in the chemical composition.

1. Introduction

Aluminium (Al)-Magnesium (Mg)-Silicon (Si) such as AA6061 Al alloys are important in industries as they are used for a wide variety of products and applications from truck bodies and frames to screw machine parts and structural components. It offers a range of good mechanical properties and corrosion resistance, formability, and weldability [1, 2]. It can be fabricated by most of the commonly used techniques. In addition, the alloys are desirable materials for making components of internal combustion engine such as cylinder block, cylinder head, and piston which are usually subjected to a relatively high temperature applications [3, 4].

At present, the effect of oxidation temperature on bare material or unwelded structure of Al-Mg alloy is well established. Meanwhile, when it involved a welded structure, the influence of alloying element from filler metal addition on the growth and morphology of oxide on the fused or welded surface shows a clear difference. Welding an Al represents a critical operation due to its complexity and the high level of defect that can be produced in the fused metal. The main

problems are related to the properties of Al that is high thermal conductivity, high chemical reactivity with oxygen, and high hydrogen solubility at high temperature [4, 5].

In other words, when it involved a welded structure, the oxidation process may be more complex for fused metal parts of alloys with different oxide growth rate due to (i) nature of difference of metallurgical structure from filler and parent metal and (ii) the presence of discontinuities resulting from previous welding procedure [4]. It is not a simple system because slightly different adsorption and surface conditions could lead to significant differences in the resultant reaction. The oxidation kinetics of a metal or alloy was determined by a number of processes which are atomic transport through the oxide layer and reactions at one or both interfaces (metal oxide layer and oxide gas) [5]. The resistance of a metal attack by aggressive gasses is primarily related to the protective properties of the surface oxide layer.

A study by Maggiolino and Schmid [4] showed that at temperatures of more than 500°C, oxide formed on 6000 series Al alloy surface has resulted in a very significant weight gain which means more metal loss and degradation

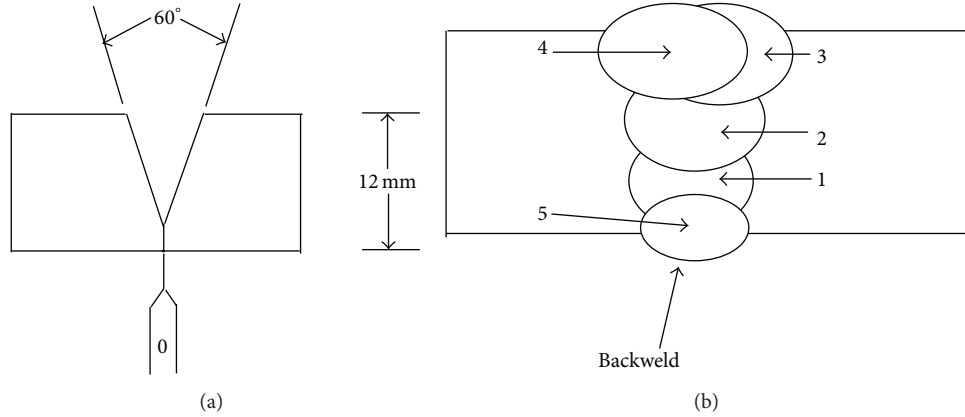


FIGURE 1: Welding details of AA6061 Al alloy plates: (a) joint configuration and (b) welding sequence, 1 → 2 → 3 → 4 → 5 (backweld).

TABLE 1: Chemical composition in wt% of base metal AA6061 Al alloy and filler metal ER5356.

	Si	Fe	Cu	Mn	Mg	Cr	Zn	Ti	Al
AA6061	0.8	0.7	0.4	0.15	1.2	0.35	0.25	0.15	96.10
ER5356	0.27	0.40	0.10	0.10	5.00	—	—	—	94.13

of its mechanical properties [5–7]. Frolich et al. [7] reported that the oxide scale formed on Al alloys has been more tenacious which led to the intermixing of the surface metal and oxide scale leading to a complex surface and subsurface layer. It is well known that Mg which is one of the common alloying elements for Al alloy has high affinity to oxygen and is particularly prone to surface degradation during high temperature manufacturing stages such as welding or heat treatment [8–11]. van Agterveld et al. [1] reported that the Al-Mg alloy exposed up to 400°C in an air circulation furnace formed surface oxide layer largely consisting of MgO.

In this present work, a study was conducted on the oxide scale formed on the fused metal part of AA6061 welded joint that was subjected to high temperature oxidation test. The nature of the oxide growth pattern, morphology, and phases was characterized using scanning electron microscope (SEM) equipped with energy dispersive X-ray spectroscopy (EDS) and X-ray diffraction (XRD) technique. In the present investigation, the X-ray photoelectron spectroscopy (XPS) was applied to get more information on the preferential interaction of the formed oxide.

2. Material and Methods

Samples used for high temperature oxidation test were AA6061 welded alloy focusing only on the fused metal part prepared by means of gas metal arc welding (GMAW) technique operating at 25 V and 185 A, using commercially available filler metal ER5356 (Al-5Mg). Table 1 shows the chemical composition of the base and filler metals. The welding parameters used to join AA6061 alloy plate is shown in Table 2. Figure 1 shows the joint configuration and sequence of welding process used in this work.

TABLE 2: Welding parameters used to weld AA6061 Al alloy.

Welding parameter	Description
Diameter filler wire ER5356	1.00 mm
Polarity	Direct current reverse polarity (DCRP)
Amperage	185 A
Voltage	25 V
Travelling speed	400 mm/min
Heat input	0.75 ± 0.08 KJ/mm
Shielding gas	Argon

The AA6061 Al alloy plates had original dimension of 300 mm (length) × 200 mm (width) × 12 mm (thick) with single-V groove butt joint. Following the welding procedure, the bead contour, bead appearance, and weld quality have been inspected visually to identify the discontinuities of the fused metal part. Then, samples with dimension of 60 mm (length) × 10 mm (width) × 5 mm (thick) were cut from the welded plate comprising of base and fused metal parts. The samples were mechanically grinded using silicon carbide papers and followed by polishing with 3 μ and 1 μ diamond paste. These samples were utilized for high temperature oxidation test. The oxidation test was carried out using a laboratory type air circulated horizontal tube furnace at 600°C in air atmosphere for the duration of 8, 20, 30, and 40 hours followed by a slow cooling rate of 1.5°C min⁻¹. The samples weight before and after oxidation test were determined by using an electronic balance with an accuracy of ±0.001 mg.

Although the oxidation test was studied for 600°C at all duration exposures which are 8, 20, 30, and 40 hours, the characterization analysis was evaluated only for sample undergone oxidation for 40 hours. The oxidized fused metal samples were then characterized using a scanning electron microscope (SEM) LEO 1450 model equipped with an energy dispersive X-ray spectroscopy (EDS) to obtain oxide scale morphology, cross-sectional images, and the constituent

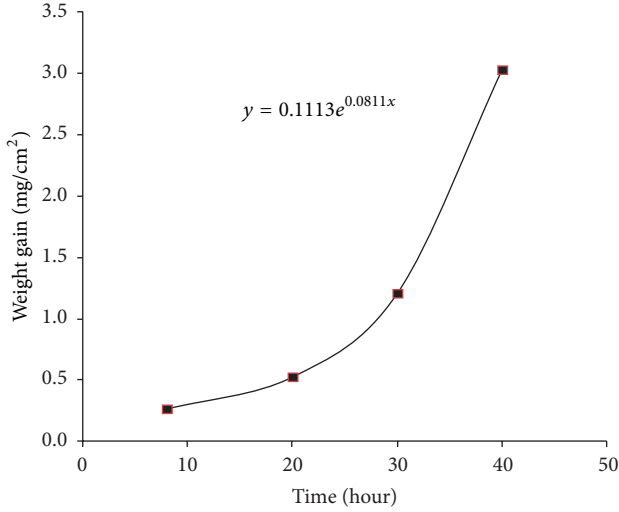


FIGURE 2: Weight gain per unit surface area versus time for welded AA6061 Al alloy sample heated at 600°C.

element present. Phase identification was carried out using X-ray diffractometer (XRD) Bruker AXS:D8 Advance model.

The evolution of the chemical composition, mainly the depth distribution of various chemical species within the grown oxide scales on fused metal, was studied by using X-ray photoelectron spectroscopy (XPS) Axis Ultra model. The spectra were taken with the Al K α X-ray source operating at 400 W (15 kV-27 mA). The fused metal samples were analyzed at an electron take-off angle of 70°, measured with respect to the surface plane. XPS spectrum analysis was performed by peak fitting employing the respective procedures using the data system analysis. During data fitting, a Shirley background correction was applied to all spectra. In order to identify the elements present, a high resolution broad scan survey spectrum is obtained.

3. Results and Discussion

3.1. Kinetics of Oxidation. The overall weight gain per unit area of AA6061 welded Al alloy, W , including both base and fused metal parts due to the formation of oxide was calculated using the following:

$$\left(\frac{\Delta W}{A}\right)_{\text{WD}} = \frac{W_f - W_i}{A}, \quad (1)$$

where ΔW is the overall weight gain of the welded sample (mg), W_i and W_f represent the sample's weight before and after heating, and A is surface area of the sample (cm²).

In this part, the analyses were focused on the samples which exposed to the temperature of 600°C at all exposure durations which are 8, 20, 30, and 40 hours. At 600°C, the weight gain of sample due to the formation of oxide increased drastically after heating for more than 30 hours as shown in Figure 2. This statement is in agreement with the optical images in Figure 3 and surface micrograph of oxidized fused metal sample as indicated in Figure 5. The oxide growth

rate seems to follow an exponential equation, shown by the following:

$$\frac{\Delta W}{A} = Ce^{kt}, \quad (2)$$

where ΔW is the overall weight gain (mg), A is surface area (cm²), t is exposure time (hours), and k and C are constants [5, 12].

3.2. Oxide Scale Characterization. Figure 3 shows the optical and macrostructure images of the AA6061 welded Al alloy before being subjected to oxidation test. Figure 3(b) indicated the macrostructure image of welded joint showing the sequence of weld layers. It shows the presence of imperfection such as pore resulting from previous welding process. It is believed that the formation of porosity is caused by the absorption of gases such as oxygen, or hydrogen in the molten weld pool which is then released during solidification and becomes trapped in the weld metal [4].

Figure 4 shows the welded sample after oxidation process being set at 600°C for 40 hours duration. Compared to the nonoxidized sample in Figure 3(a), it shows the color of the welded samples especially in fused metal part turning from the metallic-like appearance to grayish black after exposure at 600°C (Figure 4) as the impact of oxidation process. From the results, it clearly implies that the oxidation temperature has a strong effect on the appearance and the oxidation behavior.

Figures 5(a) and 5(b) show the SEM images of fused metal part before and after being subjected to oxidation test at 600°C for 40 hours. The changes of appearance due to oxidation were supported by the SEM micrograph shown in Figure 5(b) indicating the formation of oxide scale on the sample's surface. It was found that, at 600°C, the oxidized fused metal surface was found to be distributed by flake-like white grains, eventually proving the color changes from the grayish black oxides to white flake-like oxides surface. The distribution of oxides was uneven. As discussed earlier, the oxidized fused metal surface was covered with agglomerated oxide grains forming a porous structure. This oxides formation supports the experimental result that the grown oxide or weight gain in welded AA6061 Al alloy at 600°C increased with time exponentially (Figure 2).

The enrichment of elements was significantly shown in cross-sectional analyses with EDS maps of oxidized and nonoxidized fused metal part in Figures 6 and 7, respectively.

The oxides enrichment that contained Al, Mg, Si, and O was found to be scattered evenly in Figure 6 indicating that the sample was free from oxidation exposure. On the other hand, an enrichment of oxides was found to be distributed unevenly especially at the oxide-alloy interface of oxidized fused metal part as shown in Figure 7. It was found that the outer oxide scale was thick and porous. In the internal part of the sample's substrate, the oxide nodule was formed and the EDS maps analyses confirmed an enrichment of oxides that contained Mg and Si.

Meanwhile, the XRD scan of oxidized and nonoxidized sample was shown in Figures 8(a) and 8(b). Figure 8(a) shows the unoxidized fused metal surface of AA6061 welded Al

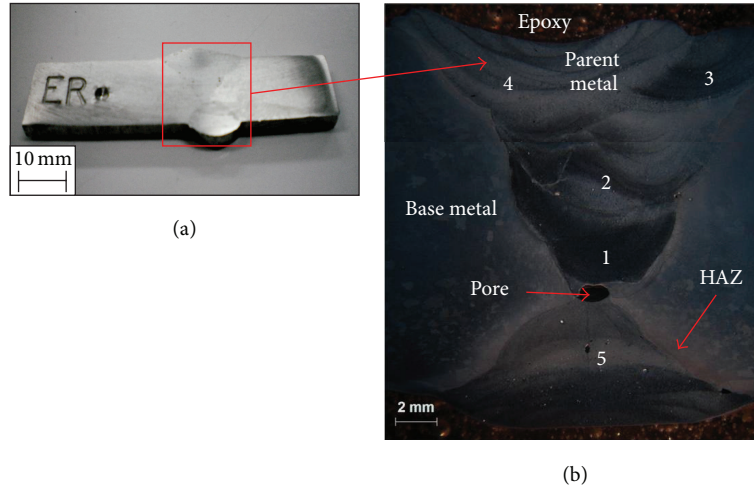


FIGURE 3: AA6061 welded sample before being subjected to oxidation test consisting of (a) optical image and (b) macrostructure showing parent, fusion metal, and heat affected zone (HAZ).

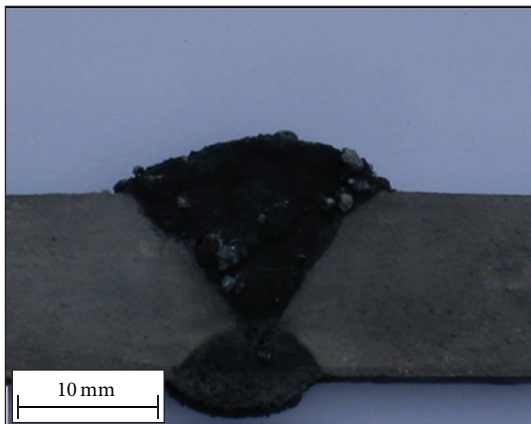


FIGURE 4: Optical image of oxidized AA6061 welded sample consisting of parent and fusion metal for 40 hours at 600°C.

alloy. The XRD spectrum shows the presence of Al and δ - Al_2O_3 . Meanwhile, the XRD scan detected the presence of phases such as δ - Al_2O_3 , γ - Al_2O_3 , and MgO as shown in Figure 8(b). MgO phases had been detected with low peaks of intensity and did not exhibit a broadening behavior. The patches of Mg-rich oxides present in the oxidized samples shown by SEM micrographs and EDS maps analyses (Figure 7), possibly from MgO. At 600°C the presence of Al-rich oxides is more significant instead of oxides that contained Mg and Si due to the presence of γ - Al_2O_3 and δ - Al_2O_3 (Figure 8). Moreover, it is believed that the presence of MgO spectrums (Figure 8(b)) was due to a higher diffusion rate of Mg^{2+} and Al^{3+} into MgO.

3.3. Chemical State of the Ions. Further analysis of oxide formation on the surface of fused metal part was confirmed by XPS analysis in Figure 9 since the details of oxide

formation were not fully justified in XRD scan (Figure 8). The analysis was only carried out for oxidized welded sample at 600°C for 40 hours. A wide XPS spectrum shows that the sample contains the species of Si 2p, Mg 2p, Al 2p, C 1s, and O 1s which is clearly seen in the survey. High resolution of O 1s, Mg 2p, Si 2p, and Al 2p of the fused metal oxide surface is shown in Figure 10. The XPS survey spectra showed Al, Mg, Si, O, and C to be the main elements with other elements only appearing at trace levels. The graph profile shown is corrected for sample charging effects, where the spectra were shifted to set the C-C component of the C 1s core level peak at a binding energy of 284.8 eV.

It is emphasized in previous literature [10–14] that oxygen molecules approaching the Al surface have two major possibilities in surface interaction. In that case, either they are dissociated in the vicinity of the surface by a charge transfer into the oxygen antibonding molecular orbital or otherwise the whole oxygen molecule is reflected from the surface [15]. The O 1s BE of 533.03 ± 0.08 eV for the O 1s main peak in Figure 10(d) can be compared with the corresponding O 1s BE of 531.8 ± 0.5 eV and 531.2 ± 0.3 eV, as reported for bulk and thin films of MgO and MgAl_2O_4 by Jeurgens et al. [13]. It also corresponds to the formation of γ - Al_2O_3 and SiO_2 α -quartz with BE of 533.83 ± 0.02 eV.

In order to measure the various binding energy positions, the graph profile was determined accurately by fitting of a third degree polynomial function through the top of the respective peaks. The two Al species was observed in Figure 10(a). The Al 2p binding energy (BE) value of 74.05 ± 0.1 and 72.3 ± 0.1 eV of the interfacial oxide scale species in (Figure 10(a)) lies in between 72.9 ± 0.1 and 74.3 ± 0.1 eV as reported for thin γ - Al_2O_3 films and Al was observed in [13]. It is noted in previous literature that this BE value (i.e., 74.05 eV) is slightly higher than the corresponding Al 2p BE value of 74.0 ± 0.1 eV as reported by Jeurgens et al. [13] for Al cations. It has been previously reported that the BE of the Al 2p for Al_2O_3 is 74.4–75.8 eV [13]. It is suggested that the interfacial

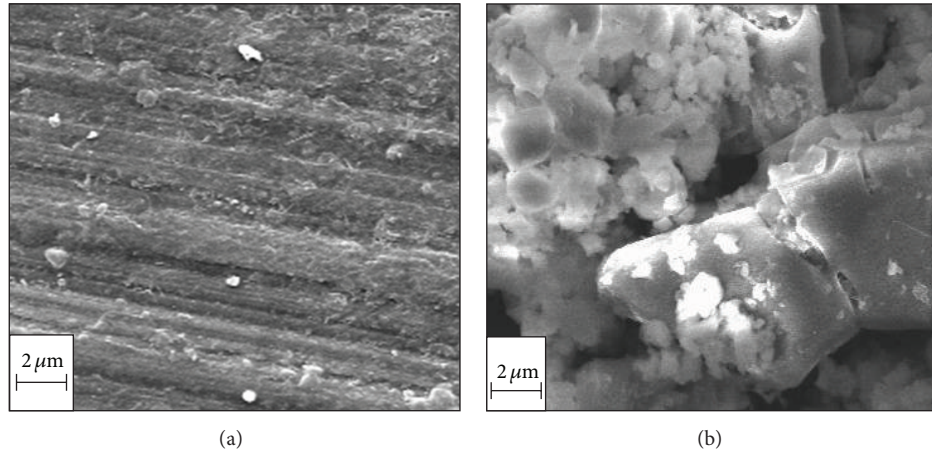


FIGURE 5: SEM micrograph of fused metal surface oxide morphology, (a) before and (b) after being subjected to oxidation test for 40 hours at 600°C.

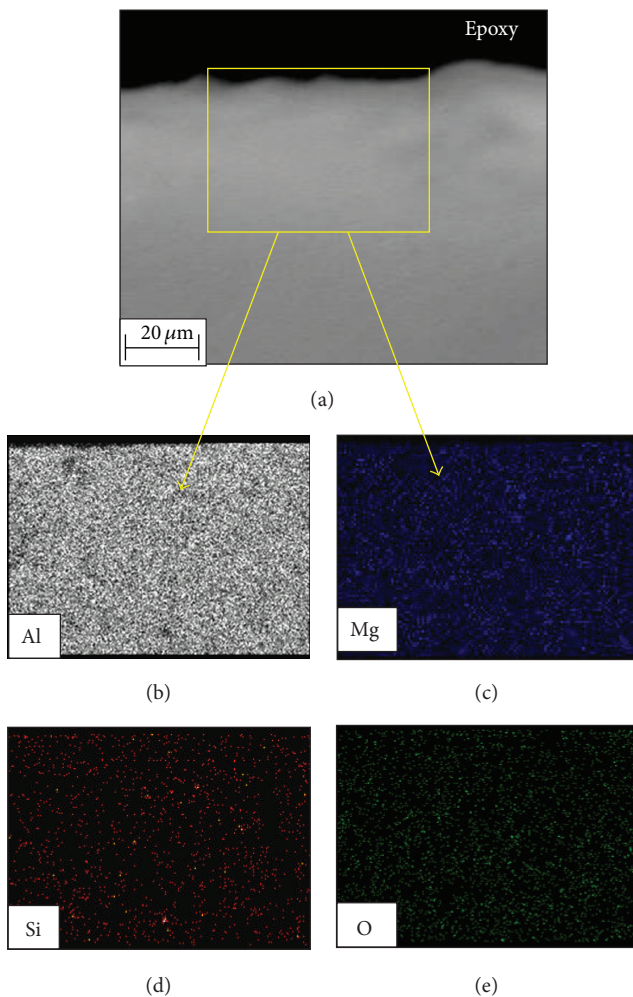


FIGURE 6: A cross-sectional image of nonoxidized fused metal part of welded AA6061 Al alloy, (a) SEM image, and EDS maps analyses of (b) Al, (c) Mg, (d) Si, and (e) O.

Al cations that give rise to the Al 2p species in the grown oxide scale, are in their formal oxidation state which is Al^{3+} . Its chemical environment possesses the similarity of those Al cations in Al_2O_3 and/or $MgAl_2O_4$ as reported in [16].

The Mg 2p BE of 50.41 ± 0.1 eV for the grown oxide scale in Figure 10(b) complies well with the corresponding BE value of 50.4 ± 0.3 eV for bulk and thin film of $MgAl_2O_4$ [17]. The second species of Mg 2p BE of 52.17 ± 0.1 eV was confirmed to the compound of MgO. It is slightly higher than the corresponding Mg 2p BE of 50.8 ± 0.3 eV as reported for bulk and thin film of MgO [18]. Figure 10(c) shows an XPS spectrum in the Si 2p energy region for an oxidized fused metal sample. It is observed that there were two Si species observed using the peak convolution method. The Si peaks deconvoluted at 100.28 ± 0.1 eV and 103.6 ± 0.1 eV were expressed as Si 1 and Si 2, respectively. The Si 2p peak which is assigned as Si 1 with the BE of 100.2 ± 0.1 eV was considered to be due to the formation of Si n-type and the Si 2 peak with a different binding energy of 103.6 ± 0.1 eV was found to be due to SiO_2 . In Figure 10(c), the phase separation of oxide states of Si 2p is taking place. At higher temperature, possible formation mechanism involves the exchange of oxygen and Si leading to the formation of SiO_2 .

3.4. Thermodynamics of Oxidation. According to the thermodynamics considerations, the Gibbs free-energy change for the formation of a compound, ΔG , is commonly represented as

$$\Delta G = \Delta H - T\Delta S, \quad (3)$$

where ΔH is the enthalpy change and ΔS is the entropy change in a system.

The calculated values, ΔG , of possible phases that formed after oxidation at temperatures of 600°C for 40 hours are listed in Table 3. The ΔG_{600}° for the formation of MgO at 600°C using 1 mol of O_2 was equal to $-1,015.68$ kJ which is lower

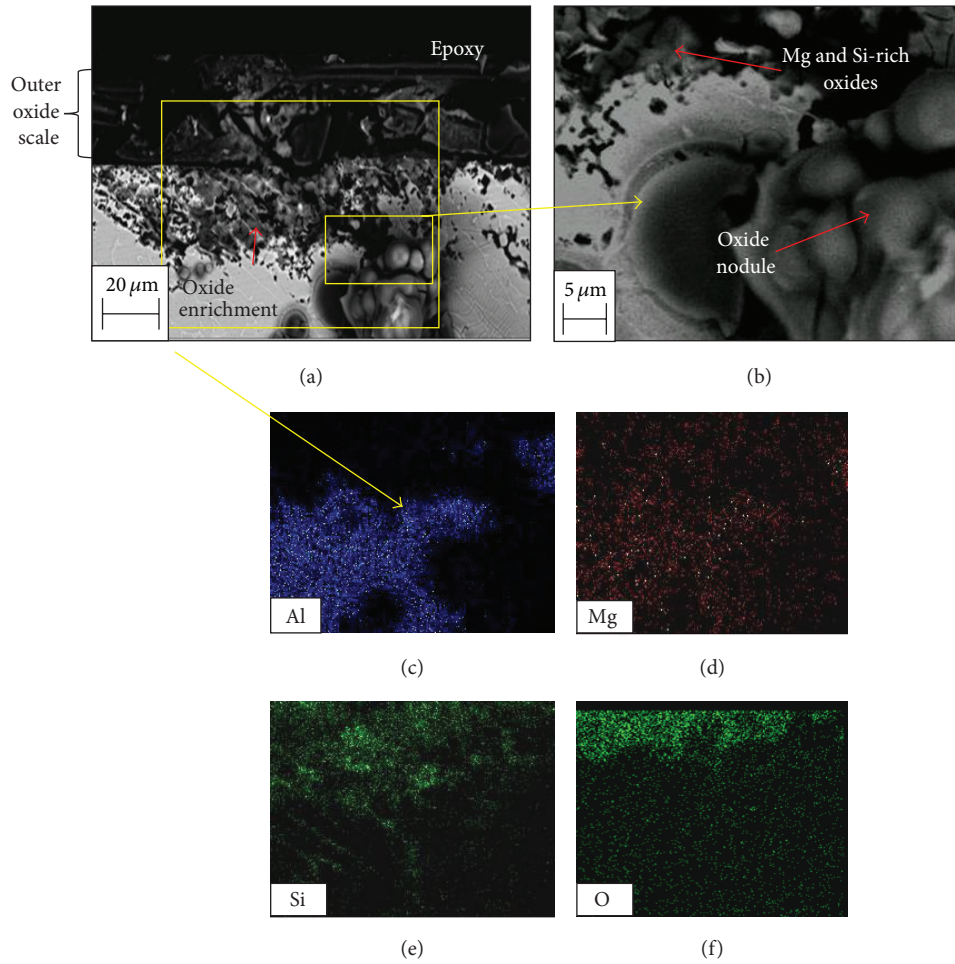


FIGURE 7: A cross-sectional image of fused metal part of welded AA6061 Al alloy oxidized at 600°C for 40 hours, (a) SEM image and (b) expanded SEM image in (a) and EDS maps analyses of (c) Al, (d) Mg, (e) Si, and (f) O.

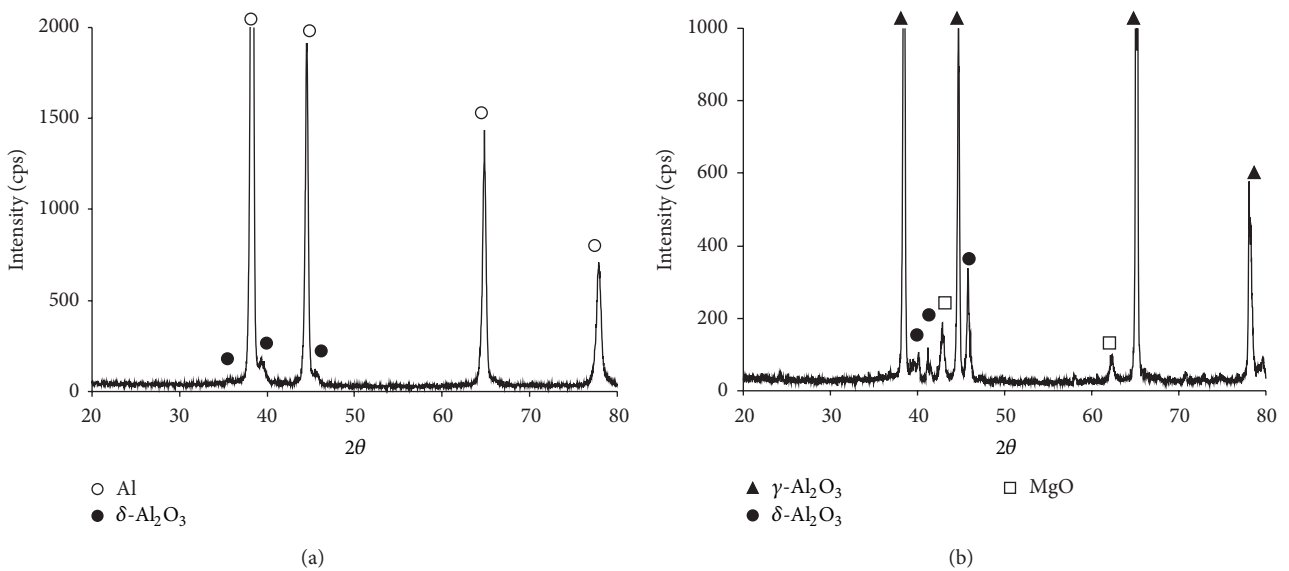


FIGURE 8: XRD diffractograms of fused metal surface of welded AA6061 Al alloy, (a) before and (b) after being subjected to oxidation test for 40 hours at temperature of 600°C.

TABLE 3: The possible chemical reaction and standard Gibbs free energies during oxidation at 600°C.

Reaction	$-\Delta H$ (J/g.mole)	$-\Delta S$ (J/g.mole.°K)	ΔG_{600}° (kJ)
$2\text{Mg} + \text{O}_2(\text{g}) \rightarrow 2\text{MgO}$	1,219,140	233.04	-1,015.68
$(0.5)\text{Mg} + \text{Al} + \text{O}_2(\text{g}) \rightarrow (0.5)\text{MgAl}_2\text{O}_4$	1,164,035	218.84	-972.98
$4/3 \text{Al} + \text{O}_2(\text{g}) \rightarrow 2/3 \text{Al}_2\text{O}_3$	1,121,922	215.47	-931.66
$2\text{Mg} + \text{Si} \rightarrow \text{Mg}_2\text{Si}$	155,600	-75.0	-90.12

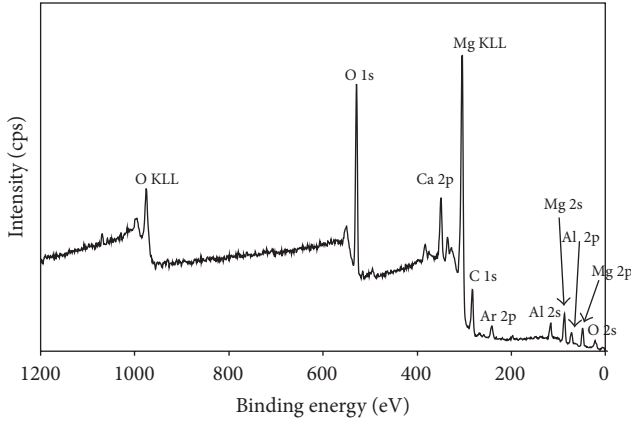
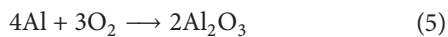


FIGURE 9: The wide XPS spectra of oxidized fused metal surface of AA6061 welded Al alloy at 600°C for 40 hours exposure duration.

than those for MgAl_2O_4 (-972.98 kJ) and Al_2O_3 (-931.66 kJ). Therefore, it is suggested that the order of priority of the reactions is as follows: (1) Mg was oxidized to MgO, (2) Mg and Al were oxidized to MgAl_2O_4 , and (3) Al was oxidized to Al_2O_3 .

Earlier, the presence of $\delta\text{-Al}_2\text{O}_3$ and $\delta\text{-Al}_2\text{O}_3$ via XRD, EDS, and XPS was confirmed. Initially, a thin Al_2O_3 layer was formed on the surface of the fused metal at room temperature and at the beginning of heating which naturally prevents the alloy surface from corrosion reaction. Al_2O_3 is a protective layer which is initially impermeable to water vapour or gases [17–19]. Further heating may lead oxygen to diffuse into the oxide and reach the surface of fused metals.

Then, a new oxidation process started to take place on the oxide-alloy interface to form a new oxide, separating the previously formed oxide from the alloy. Equations (4) to (8) are an example of the possible reactions that may happen during oxidation reactions:

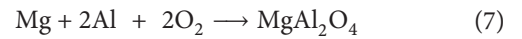


The above oxidation reactions are exothermic ($\Delta H < 0$) as shown in Table 3. The oxide formed leads the samples to experience weight gain. The oxides then formed MgAl_2O_4 through a solid state reaction according to (6) [18–22]. This process involves interdiffusion of Al^{3+} and Mg^{2+} ions into MgO and Al_2O_3 . It is reported that MgAl_2O_4 is hard and porous [23, 24]. MgAl_2O_4 may also nucleate and grow on the

alloy-oxide interface via a direct reaction of Al and Mg with O_2 as shown by the following [25]:



or



It is suggested that the influence of Mg as an alloying element from the addition of filler metal on the oxidation resistance is mainly to lower the defect associated in the Al_2O_3 layer as discussed by Nylund et al. [12]. It has been shown that small amounts of Mg added to Al will decrease the oxidation rate. On the other hand, contradicting results were observed when it involved a welded structure that previously experienced solidification process during welding. Moreover, the oxide layer that formed on Al below 400°C is amorphous and it is clearly investigated that the growth of the amorphous oxide follows an inverse logarithmic rate law [18, 20, 23]. In Cabrera and Mott theory, thin films grow at low temperatures predominantly by cation migration and influenced by potential accumulation across the growing film. At an initial stage, the alloy and oxygen reaction mechanism involves the adsorption of gas on the alloy surface [26].

It can be explained that the details of the formation of MgAl_2O_4 occur either by the reaction between Al_2O_3 layers grown with Mg in the alloy or by solid state reaction between MgO phases which grows out of an alloy with internal Al_2O_3 layer. This is in line with those reported by Shimizu et al. [20]. Both phases, namely, MgAl_2O_4 and MgO, are metastable. Overall, this shows that during the reaction, Mg-rich oxide is formed. During the process of oxide scale growth, the rapid reaction occurs in which the MgO moves out towards the oxide-gas interface. At the bottom layer a form of MgAl_2O_4 from the reaction of Mg-Al-O or MgO and Al_2O_3 layer thickening with increasing temperature. Since the Mg depleted, it is believed that the low compound of MgO was formed since Mg is prone to precipitate with Si according to the following:



With further oxidation, the movement of cation spread to the oxide-gas interface causes Al_2O_3 grows towards the surface. At one time, the growth of Al_2O_3 is depleted, thus slowing down the oxide growth. At this point Al is reduced, and further oxidation of Al_2O_3 could not continue [12, 27]. In this case, the growth of the nonprotective $\text{MgAl}_2\text{O}_4/\text{MgO}$ and precipitation of Mg and Si on the fused metal surface is significantly pronounced.

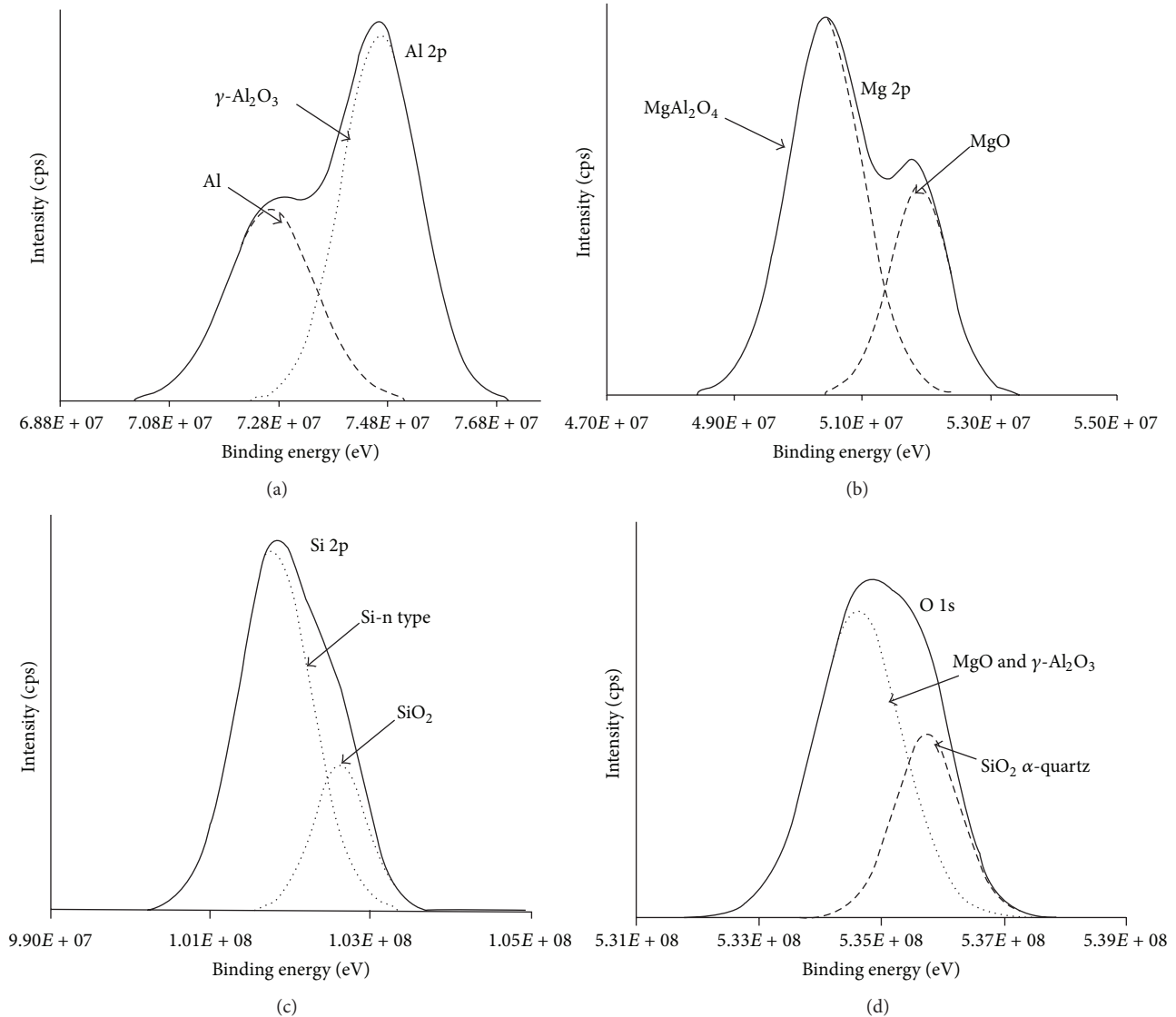


FIGURE 10: The detail profile of XPS scan (a) Al 2p, (b) Mg 2p, (c) Si 2p, and (d) O 1s signals of oxidized fused metal part of AA6061 welded Al alloy at 600°C for 40 hours exposure duration.

Particularly, the unique zone between fused and non-fused base metal which known as fusion boundary were found to be the critical and complex parts where all element compositions lying within the fusion boundary were a mixture of filler and base metal alloys. Pure metals and alloys are not stable especially when it has been exposed to a high temperature oxidation environment [28, 29]. In the case of welded part, a combination of high temperature and oxidation environment with contaminants resulting from previous welding procedure might lead to the internal degradation at a very rapid rate [30, 31]. Porosity defect in fused metal part also increased the penetration of oxygen which in turn acts as a channel that accelerates the oxidation process. Defects resulting from the welding process and during sample preparation were found to play an important role in assisting the oxidation process. Porosity and voids could increase the rate of oxygen entry into the welded alloy

surface and therefore would act as a quick channel or a short pathway for oxidation took place.

According to Arranz and Palacio [28], there is a controversy on the mechanisms of oxygen chemisorptions and nucleation and growth of the surface oxide on single-crystal Al surfaces. They showed that the interaction of oxygen with Al works in two different ways, either the formation of surface and subsurface species during oxygen adsorption or the simultaneous formation of two-layer oxygen islands and single-layer oxygen islands. The dynamic changes of the chemical state in high temperature oxidation revealed that the Al substrate containing Mg will cause the Mg to be distributed in the matrix and move to the surface. Thus, this process will lead to the concentration of Mg and reduce the aluminum oxide. It is in agreement with Kimura et al. [29] showing that the result indicates that the appearance of the metallic state was due to the growth of alumina crystallites between the

surface oxide layer and inner metallic region. It shows that only Mg concentrated in the oxide layer can reduce the Al_2O_3 . Consequently, the main oxide entrapped in welded Al alloy is MgO. It was found to be in agreement with Chen and Wei [30] that the main phases of the oxide films are MgO and MgAl_2O_4 . MgAl_2O_4 was recorded to have a low free energy so that it is often formed at the interface of the Al matrix and MgO. Thus, the mechanism involved is basically based on the diffusion of a solute Al to the interface to react with oxygen and MgO. It was noted that MgAl_2O_4 is more brittle than MgO. The oxides that are entrapped in welded Al alloy show that it is rich in Al, Mg, and O. The oxide can serve as a stress raiser where nucleation site takes place. This oxide surface will thus act as a nucleation site for the formation of pores or inclusions in welded Al alloy.

According to Do et al. [31], it is evident that the addition of Si or Mg in Al bare material will result in an increase or reduction in the number of defects in the oxide scale and therefore lead to the changes in oxidation kinetics. They proved the change of Mg activity in the Al_2O_3 related to the formation of new phase which is a nucleation of a MgAl_2O_4 . From this investigation, there is a large volume change associated with the transformation from MgO to MgAl_2O_4 [31]. The formation of rapidly growing breakaway-type, MgAl_2O_4 -rich oxides, comes from the fact that Mg oxidized internally rather than forming a protective external scale. The mechanism is expected to be promoted by the direct reaction of air gas with alloy surface through a porous surface that contained voids and pores.

4. Conclusion

The oxide formed on the fused metal part of AA6061 Al alloy which was joined by gas metal arc welding using an addition of Al-5Mg filler metal; ER5356 was grayish black in color and degrade faster when subjected to high temperature oxidation at 600°C for 40 hours. The oxide growth rates based on weight gain at 600°C have followed exponential functions. At 600°C , the oxidation process induces segregation of Mg from the alloy's interior to the alloy-oxide interface. These segregated Mg cations incorporated into the oxide which gives rise to the occurrence of MgO as confirmed by XRD, EDS, and XPS. As long as the grown oxide continued to thicken, Mg interfacial segregation became larger at 600°C . The oxidation mechanism AA6061 Al alloy welded joint represents a complex process involving several exothermic reactions which produced $\delta\text{-Al}_2\text{O}_3$, $\gamma\text{-Al}_2\text{O}_3$, MgO, and MgAl_2O_4 . In addition, XPS results have been found to be consistent with the interpretation of the existence of oxide phases which grow and cover the surface completely.

Conflict of Interests

The authors declare that there is no conflict of interests regarding the publication of this paper.


Acknowledgments

The authors would like to thank the Ministry of Higher Education Malaysia and Universiti Kebangsaan Malaysia (UKM) for supporting this work through research Grants FRGS/1/2011/ST/UKM/02/14, UKM-GGPM-NBT-089-2010, DIP-2012-14, DPP-2013-035, and STRG1033. One of the authors, Nur Azida Che Lah, would like to thank Universiti Kuala Lumpur Malaysia France Institute (Unikl MFI) and Majlis Amanah Rakyat (MARA) for granting a fellowship for her doctoral study. The authors kindly declare that "Submission of the article implies that the work describe has not been published elsewhere."

References

- [1] D. T. L. van Agterveld, G. Palasantzas, and J. Th. M. De Hosson, "Magnesium surface segregation and oxidation in Al-Mg alloys studied with local probe scanning Auger-scanning electron microscopy," *Applied Surface Science*, vol. 152, no. 3, pp. 250–258, 1999.
- [2] F. Andreatta, H. Terryn, and J. H. W. De Wit, "Corrosion behaviour of different tempers of AA7075 aluminium alloy," *Electrochimica Acta*, vol. 49, no. 17-18, pp. 2851–2862, 2004.
- [3] E. Arslan, Y. Totik, E. E. Demirci, Y. Vangolu, A. Alasaran, and I. Efeoglu, "High temperature wear behavior of aluminum oxide layers produced by AC micro arc oxidation," *Surface and Coatings Technology*, vol. 204, no. 6-7, pp. 829–833, 2009.
- [4] S. Maggolino and C. Schmid, "Corrosion resistance in FSW and in MIG welding techniques of AA6XXX," *Journal of Materials Processing Technology*, vol. 197, no. 1–3, pp. 237–240, 2008.
- [5] A. F. Beck, M. A. Heine, E. J. Caule, and M. J. Pryor, "The kinetics of the oxidation of Al in oxygen at high temperature," *Corrosion Science*, vol. 7, no. 1, pp. 1–22, 1967.
- [6] G. C. Wood and F. H. Stott, "Oxidation of alloys," *Materials Science and Technology*, vol. 3, no. 7, pp. 519–530, 1986.
- [7] M. F. Frolich, M. Krzyzanowski, W. M. Rainforth, and J. H. Beynon, "Oxide scale behaviour on aluminium and steel under hot working conditions," *Journal of Materials Processing Technology*, vol. 177, no. 1-3, pp. 36–40, 2006.
- [8] F. Reichel, L. P. H. Jeurgens, and E. J. Mittemeijer, "The effect of substrate orientation on the kinetics of ultra-thin oxide-film growth on Al single crystals," *Acta Materialia*, vol. 56, no. 12, pp. 2897–2907, 2008.
- [9] U. K. Mudali and B. Raj, *Corrosion Science and Technology*, Alpha Science International, 2008.
- [10] F. Czerwinski, "The oxidation behaviour of an AZ91D magnesium alloy at high temperatures," *Acta Materialia*, vol. 50, no. 10, pp. 2639–2654, 2002.
- [11] V. V. Doilnitsyna, "General diffusion-kinetic model of metallic oxidation," *Corrosion Science*, vol. 44, no. 5, pp. 1113–1131, 2002.
- [12] A. Nylund, K. Mizuno, and I. Olefjord, "Influence of Mg and Si on the oxidation of aluminum," *Oxidation of Metals*, vol. 50, no. 3-4, pp. 309–325, 1998.
- [13] L. P. H. Jeurgens, M. S. Vinodh, and E. J. Mittemeijer, "Initial oxide-film growth on Mg-based MgAl alloys at room temperature," *Acta Materialia*, vol. 56, no. 17, pp. 4621–4634, 2008.
- [14] C.-S. Yang, J.-S. Kim, J.-W. Choi et al., "XPS study of aluminum oxides deposited on PET thin film," *Journal of Industrial and Engineering Chemistry*, vol. 6, no. 3, pp. 149–156, 2000.

- [15] J. F. Moulder, W. F. Stickle, P. E. Sobol, and K. D. Bomben, *HandBook of X-Ray Photoelectron Spectroscopy, A Reference Book of Standard Spectra For Identification and Interpretation of XPS Data*, Perkin-Elmer Corporation, Waltham Mass, USA, 1992.
- [16] M. Frerichs, F. Voigts, and W. Maus-Friedrichs, "Fundamental processes of aluminium corrosion studied under ultra high vacuum conditions," *Applied Surface Science*, vol. 253, no. 2, pp. 950–958, 2006.
- [17] J. A. S. Tenório and D. C. R. Espinosa, "High-temperature oxidation of Al-Mg alloys," *Oxidation of Metals*, vol. 53, no. 3, pp. 361–373, 2000.
- [18] H. Venugopalan, K. Tankala, and T. DebRoy, "Kinetics of directed oxidation of Al-Mg alloys in the initial and final stages of synthesis of $\text{Al}_2\text{O}_3/\text{Al}$ composites," *Materials Science and Engineering A*, vol. 210, no. 1-2, pp. 64–75, 1996.
- [19] N. Arivazhagan, S. Singh, S. Prakash, and G. M. Reddy, "High temperature corrosion studies on friction-welded dissimilar metals," *Materials Science and Engineering B*, vol. 132, no. 1-2, pp. 222–227, 2006.
- [20] K. Shimizu, G. M. Brown, K. Kobayashi, P. Skeldon, G. E. Thompson, and G. C. Wood, "The early stages of high temperature oxidation of an Al-0.5 wt% Mg alloy," *Corrosion Science*, vol. 40, no. 4-5, pp. 557–575, 1998.
- [21] N. K. Othman, N. Othman, J. Zhang, and D. J. Young, "Effects of water vapour on isothermal oxidation of chromia-forming alloys in Ar/O_2 and Ar/H_2 atmospheres," *Corrosion Science*, vol. 51, no. 12, pp. 3039–3049, 2009.
- [22] N. K. Othman, A. Jalar, N. Othman, and D. J. Young, "Effects of lanthanum on Fe-25Cr alloys under cyclic oxidation," *Advanced Materials Research*, vol. 97–101, pp. 1212–1215, 2010.
- [23] V. Y. Chekhovskoi and V. D. Tarasov, "A procedure for rapid studies of the metal oxidation kinetics at high temperatures," *Instruments and Experimental Techniques*, vol. 51, no. 3, pp. 476–479, 2008.
- [24] S. Chevalier, C. Nivot, and J. P. Larpin, "Influence of reactive element oxide coatings on the high temperature oxidation behavior of alumina-forming alloys," *Oxidation of Metals*, vol. 61, no. 3-4, pp. 195–217, 2004.
- [25] E. Bergsmark, C. J. Simensen, and P. Kofstad, "Oxidation of molten aluminium," *Materials Science and Engineering A*, vol. A120-1, no. 1, pp. 91–95, 1989.
- [26] H. Jafari, M. H. Idris, and A. Ourdjini, "High temperature oxidation of AZ91D magnesium alloy granule during in-situ melting," *Corrosion Science*, vol. 53, no. 2, pp. 655–663, 2011.
- [27] P. Kofstad, *High Temperature Corrosion*, Elsevier, London, UK, 1988.
- [28] A. Arranz and C. Palacio, "Characterization of the surface and interface species formed during the oxidation of aluminum," *Surface Science*, vol. 355, no. 1–3, pp. 203–213, 1996.
- [29] A. Kimura, M. Shibata, K. Kondoh et al., "Reduction mechanism of surface oxide in aluminum alloy powders containing magnesium studied by x-ray photoelectron spectroscopy using synchrotron radiation," *Applied Physics Letters*, vol. 70, no. 26, pp. 3615–3617, 1997.
- [30] Y.-J. Chen and P.-S. Wei, "Diagnosis and analysis of oxide films in cast magnesium alloys by ultrasonic-vibration treatment," *Materials Transactions*, vol. 48, no. 12, pp. 3181–3189, 2007.
- [31] T. Do, S. J. Splinter, C. Chen, and N. S. McIntyre, "The oxidation kinetics of Mg and Al surfaces studied by AES and XPS," *Surface Science*, vol. 387, no. 1–3, pp. 192–198, 1997.



Hindawi

Submit your manuscripts at
<http://www.hindawi.com>

